

Contents lists available at ScienceDirect

Quaternary Science Reviews

journal homepage: www.elsevier.com/locate/quascirev



Different response of stalagmite δ^{18} O and δ^{13} C to millennial-scale events during the last glacial, evidenced from Huangjin Cave, northern China



Yijia Liang ^a, Kan Zhao ^{b, c, *}, Yongjin Wang ^{b, c}, R. Lawrence Edwards ^{b, d}, Hai Cheng ^e, Qingfeng Shao ^{b, c}, Shitao Chen ^{b, c}, Jinyu Wang ^{b, c}, Junji Zhu ^{b, c}

- ^a College of Geosciences, Nantong University, Nantong, 226007, China
- ^b School of Geography, Nanjing Normal University, Nanjing, 210023, China
- ^c Key Laboratory of Virtual Geographic Environment (Nanjing Normal University), Ministry of Education, Nanjing, 210023, China
- ^d Department of Geology and Geophysics, University of Minnesota, Minneapolis, MN, 55455, USA
- ^e Institute of Global Environmental Change, Xi'an Jiaotong University, Xi'an, 710049, China

ARTICLE INFO

Article history: Received 5 August 2021 Received in revised form 1 December 2021 Accepted 2 December 2021 Available online 9 December 2021

Handling Editor: Mira Matthews

Keywords: Huangjin Cave Stalagmite Oxygen and carbon isotopes Millennial-scale events Lead-lag relationship

ABSTRACT

An anti-phased relationship between Greenland Dansgaard-Oeschger (DO) and Antarctic temperature was revealed by ice core records, and the "bipolar see-saw" mechanism has since been proposed in explanation for the interhemispheric thermal redistribution. However, limited by chronology uncertainties of ice cores, particularly the ice age-gas age differences, the exact phase relationship and triggers for millennial-scale events are still in debate. Searching for proxies that could reflect both boreal and austral signals in one geological archive is therefore, a potential solution for the phase dilemma. Here, high-resolution paleoclimatic records from 55.2 to 36.5 ka BP were reconstructed using 21 ²³⁰Th/U dates and 647 sets of δ^{18} O and δ^{13} C data by one stalagmite HJ1 from Huangjin Cave, Hebei Province, northern China. Robust millennial-scale fluctuations are found in δ^{18} O and δ^{13} C time series, corresponding to DO events 8 to 14 and Heinrich 4 and 5 events within dating errors. Discrepancies exist in the structures and onsets in $\delta^{18}\text{O}$ and $\delta^{13}\text{C}$ records; that is, abrupt DO onsets in $\delta^{13}\text{C}$ data and gradual onsets in δ^{18} O. Timing of DO onsets in δ^{13} C are prior to (e.g. DO12 and DO14) or synchronous with (e.g. DO8 to DO11) those in δ^{18} O. Comparison of HJ1 δ^{18} O and bipolar ice core records suggests that the East Asian summer monsoon (EASM) is influenced by both hemispheres, but better mimics the Antarctic temperature. This suggests that the EASM is controlled by the cross equatorial airflows, and further indicates an important role of the Atlantic Meridional Overturning Circulation (AMOC) in modulating the inter-hemispheric heat gradient. However, our δ^{13} C profile strongly resembles with the Greenland δ^{18} O record on the millennial timescale, in terms of the "sawtooth" structure and the abrupt transition. This indicates that northern high-latitude climate could modulate hydro-thermal conditions in northern China, possibly via the mid-latitude westerly jet and/or the Silk Road teleconnection, which influences the vegetation/biomass changes and thereby controls stalagmite δ^{13} C values. Therefore, HJ1 δ^{18} O receives climatic signals from the Southern Hemisphere (SH) to a larger extent, while δ^{13} C captures largely the changes in the Northern Hemisphere (NH). Furthermore, comparison between calcite and ice core records shows that during DO14, temperature increases in the NH leads the SH cooling by ~120 years. However, during short-term DO events, the SH may start cooling ~150 years before the NH warming. These findings demonstrate two possibilities for the NH-SH phase relationship which are dependent on

st Corresponding author. School of Geography, Nanjing Normal University, Nanjing, 210023, China.

E-mail addresses: lucy2012_2015@163.com (Y. Liang), 09371@njnu.edu.cn (K. Zhao), yjwang@njnu.edu.cn (Y. Wang), edwar001@umn.edu (R.L. Edwards), cheng021@xjtu.edu.cn (H. Cheng), 09396@njnu.edu.cn (Q. Shao), chenshitao@njnu.edu.cn (S. Chen), 2693426407@qq.com (J. Wang), 1300306999@qq.com (I. Zhu).

the trigger location of the AMOC recovery and the "bipolar see-saw" mode is likely controlled by the oceanic processes.

© 2021 Elsevier Ltd. All rights reserved.

1. Introduction

Since the pioneering work of aligning bipolar ice core chronologies using methane by Blunier et al. (1998), numerous studies reveal the close teleconnection between Dansgaard-Oeschger (DO) in Greenland and Antarctic Isotopic Maximum (AIM) events/Antarctic (A) events in Antarctica (Blunier and Brook, 2001; EPICA Community Members, 2006; WAIS Divide Project Members, 2015). Comparison of bipolar ice core records shows an antiphased relationship between DO and the A/AIM events, referred to as the "bipolar see-saw" which is suggested to be forced by a shift in the intensity of the ocean conveyor (Broecker, 1998), especially the Atlantic Meridional Overturning Circulation (AMOC). The AMOC is believed to strongly modulate the heat redistribution between hemispheres (Stocker and Johnsen, 2003). This model also indicates the instability or the changing modes of the AMOC, however, with its trigger possibly residing in either of the hemispheres (Stocker and Johnsen, 2003).

The lead-lag problem is essential to understand the triggers for millennial-scale events during the last glacial period. Previously, abrupt climate changes in the Northern Hemisphere (NH) is found occurring prior to the Southern Hemisphere (SH) by 400-800 years, and thus the trigger for climatic events is suggested to reside in the NH (Schmittner et al., 2003; Knutti et al., 2004). Later, a study based on the high-resolution ice core (WDC) from the western Antarctica, again supports the "bipolar see-saw" relationship between the DO and AIM events, and refines a NH lead by ~200 years (WAIS Divide Project Members, 2015). Their work shows that climate changes in the NH and SH are coupled via the oceanic processes (WAIS Divide Project Members, 2015). The blocking role of the Antarctic Circumpolar Currents in transferring the DO signals to the Antarctica is further evidenced by Pedro et al. (2018). Recently, Walczak et al. (2020) found that rapid Cordileran ice sheet discharges into the North Pacific followed strong Asian monsoon but preceded the Heinrich (H) events, Antarctic warming, and CO₂ rise, again highlighting a NH lead. Alternatively, Landais et al. (2015) suggested that the interhemispheric temperature changes could be directly teleconnected by the atmosphere, and the abrupt warming in the NH was concomitant with the beginning of the cooling in the SH. Markle et al. (2017) and Buizert et al. (2018) also suggested that changes in the moisture source location in different Antarctic ice core sites were abrupt and occurred synchronously with DO warmings in Greenland, supporting an interpolar atmospheric see-saw. Besides, even another view exists that in some of the AIM events, the Antarctic climate changes lead those in the Greenland by 100-200 years; this was revealed by Raisbeck et al. (2017) through the landmark of the Laschamp event. Despite those numerous studies (Stocker and Johnsen, 2003; Weaver et al., 2003; WAIS Divide Project Members, 2015; Buizert and Schmittner, 2015), the lead-lag relationship between the NH and SH is still ambiguous.

By using the sedimentary core in the Iberian Margin, Shackleton et al. (2000) found that the planktonic δ^{18} O profile followed the Greenland temperature curve while the benthic δ^{18} O record resembled the Antarctic temperature changes; and from different proxies in one core, they discussed the relationship of interhemispheric temperature changes and their responses to the ice volume

changes. Lund et al. (2019) also applied similar methods on the Brazilian Margin cores to evaluate the lead-lag relationship between the AMOC and atmosphere CO_2 . Because their records are based on the same sample, the relative timing is only constrained by the core stratigraphy (Shackleton et al., 2000; Lund et al., 2019). Therefore, investigation into the phase relationship between the NH and SH from one geological sample could possibly avoid the ice age-gas age (Δ age) problem in bipolar ice cores. In this paper, we intend to utilize different proxies in one stalagmite sample to reveal the NH-SH phase relationship.

Stalagmite $\delta^{18}\text{O}$ records from Hulu Cave display millennial-scale oscillations in the East Asian summer monsoon (EASM) during the last glacial period, in response to the DO events and Henrich (H) events (Wang et al., 2001). Following Wang et al.'s work, numerous ²³⁰Th/U-dated Chinese stalagmites are used to study the timing, structure and transitions of millennial-scale events, and further to unravel the dynamic linkages between the EASM and SH/NH climates (Cai et al., 2006; Rohling et al., 2009; Zhang et al., 2016; Dong et al., 2018; Cheng et al., 2020, 2021). It is now clear that millennialscale monsoon intensifications one-to-one correspond to the DO warming events in Greenland, while they are anti-correlated with Antarctic cooling (e.g. Chen et al., 2016; Cheng et al., 2016). The impacts from both hemispheres on the EASM ideally suggest its role in the "bipolar see-saw" model, and sets the pre-conditions for the comparison in this paper. Another proxy in stalagmite is the carbon isotope (δ^{13} C), which has complex factors but strong potential in reconstructing paleoclimate and paleoecology (McDermott, 2004; Fairchild et al., 2006). Speleothem δ^{13} C is highly sensitive in response to changes in climate and environment through vegetation and biomass production (Dorale et al., 1992; Bar-Matthews et al., 1997; Frappier et al., 2002; Genty et al., 2003; Fleitmann et al., 2009). Besides, δ^{13} C could be a possible indicator for regional hydrology changes apart from its biological significance (Baker et al., 1997; McDermott, 2004). Even in some cases, calcite δ^{13} C shows better expressions for DO events than δ^{18} O, including the "sawtooth" structure (Genty et al., 2003; Fleitmann et al., 2009). Therefore, δ^{13} C in stalagmites, which is strongly impacted by regional climate, ecology and cave environment, could possibly be a powerful agent for capturing signals of DO events.

Here, based on stable isotope ($\delta^{18}O$ and $\delta^{13}C$) data and 230 Th/U dating results, we reconstruct paleoenvironmental changes during 55.6 and 36.6 ka BP from a stalagmite HJ1 from Huangjin Cave, Hebei Province, northern China. With our new records, we have three targets: (1) to obtain the timing and structure characteristics of millennial-scale events from DO8 to DO14; (2) to reveal dynamic responses of stalagmite proxies ($\delta^{18}O$ and $\delta^{13}C$) to climate and environmental changes; (3) to understand the phase relationship between the NH and SH.

2. Study site, material and methods

Huangjin Cave (118°38′E, 40°17′N, 510 m above sea level; Fig. S1) is situated in Qinglong Manchu Autonomous County, Hebei Province, on the eastern slope of the Yanshan Mountain. The study area consists of a well-developed underground karst system in the lower Sinian dolomite bedrock. It is the largest cave in this area, with a total length of 4 km and an area of over 50,000 m². Modern

vegetation is mainly composed of deciduous broad-leaved forest and coniferous forest, the typical C3 plants. The county is strongly influenced by temperate and monsoonal climate, characterised with cold-dry winters and hot-wet summers. Local mean annual temperature is ~9.3 °C and the mean annual precipitation is 692 mm. Nearly 72% of the annual rainfall occurs in the summer season (June to August) with less than 2% during the winter season (December to February next year) (Fig. S1). During the boreal summer, warm and moisture-rich air masses to the Huangjin Cave are introduced from the Indian Ocean (47%) and the Pacific Ocean (40%) (Fig. S2). Compared with the Pacific Ocean source, the Indian Ocean source contributes by apparently a higher proportion, suggesting a stronger impact from the Indian Ocean and the crossequatorial airflow as well. Indeed, the cross-equatorial airflow carries ~90% of the latent heat from the South Indian Ocean into the Indian sub-continent (Clemens et al., 1996), and further northward into the southeastern China, as a primary moisture source for summer precipitation at Huangjin site (Fig. S2).

Stalagmite sample HJ1 was found naturally broken in an inner cave chamber, ~2 km from the entrance, where the relative humidity is close to 100% throughout the year. The cone-shaped sample has a total length of 349 mm, with diameters ranging from 40 mm (top section) to 120 mm (bottom section) (Fig. 1a). The sample was cut along its growth axis and polished. It is composed of transparent and pure calcite, with one visible hiatus at the distance of 23 mm from the top and a shift of growth axis at 159 mm. The section from 24 mm to 349 mm was used in this work.

Subsamples (~70 mg) for 230 Th/U dating from HJ1 were hand drilled using 0.9 mm carbide dental burs. Twenty 230 Th/U dating was performed at Nanjing Normal University and one (HJ1-26) at Xi'an Jiaotong University, China. Chemical procedures for uranium and thorium separation, isotopic measurements and data calculations followed the methods described in Edwards et al. (1987), Cheng et al. (2000) and Shao et al. (2017, 2019). Liquid extracts of U/Th were measured using the Thermo Neptune multi-collector inductively coupled plasma mass spectrometer (MC-ICP-MS). All the speleothem 230 Th/U ages have 2σ analytical errors of roughly

0.1%-0.3% (Table 1). For stable isotope analyses, 647 subsamples were drilled at 0.5 mm intervals along the growth axis using dental burs. Powder samples were measured using Finnigan MAT-253 mass spectrometer coupled with a Kiel Carbonate Device at the School of Geography, Nanjing Normal University, China. All results were reported in parts per mill (%) relative to the Vienna Pee Dee Belemnite (VPDB) standard. Duplicate analyses of an international standard (NBS19) indicated long-term reproducibility, with precisions better than 0.06% for $\delta^{18}O$ and 0.05% for $\delta^{13}C$ at 1σ level. Totally 160 powder samples for trace metal analyses were drilled at a spatial resolution of 2 mm along the growth axis with carbide dental burs at Nanjing Normal University. These ~300-µg-powder samples were then dissolved into 15 ml 5% HNO₃ solution, settled overnight and filtered before measurements at Southwest University, China, Ba, Sr, and Mg were measured on a single-collector inductively coupled plasma mass spectrometry (SC-ICP-MS), and Ca on an inductively coupled plasma optical emission spectroscopy (ICP-OES). Trace metal results have analytical errors better than 2%.

3. Results

3.1. Chronology

The U and Th isotopic concentrations and ratios, and 230 Th/U dates are presented in Table 1. These samples have measured 238 U concentrations ranging from 620.9 ± 0.1 to 1316.8 ± 0.2 ppb, 232 Th concentrations from 401.0 ± 14.1 to 14160.9 ± 18.6 ppt and 230 Th/ 232 Th atomic ratios from $(601.6 \pm 3.2) \times 10^{-6}$ to $(25368.6 \pm 894.7) \times 10^{-6}$. Most of them have low 232 Th concentrations (a few thousand ppt) and high 230 Th/ 232 Th atomic ratios, leading to small initial detrital 230 Th corrections (within 100 years) (Edwards et al., 2003; Richards and Dorale, 2003). Merely three dates at the depths of 240 mm (HJ1-240), 251 mm (HJ1-255) and 335 mm (HJ1-355) are relatively dirty, with initial 230 Th corrections larger than 120 years and dating errors larger than 90 years. The replicate of HJ1-186R proves the reliability of the 230 Th/U dating result of HJ1-186 because these two dates agree well with each

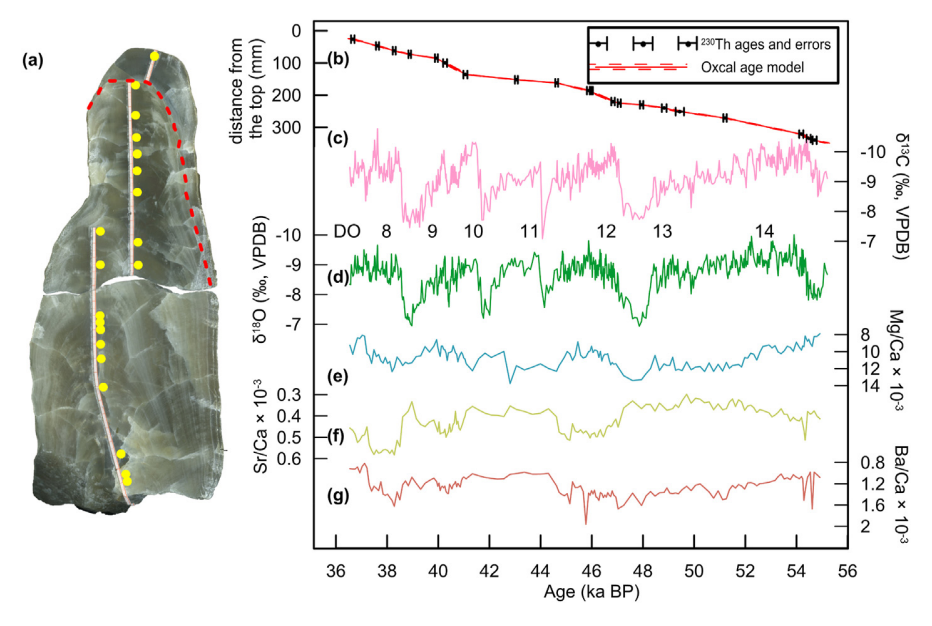


Fig. 1. Stalagmite profile, age model and multi-proxy records for the stalagmite HJ1. Left: (a) Polished profile for stalagmite HJ1, with yellow dots indicating 230 Th/U dates positions and the red dashed line indicating the visible hiatus. Right: (b) modeled ages and 2σ uncertainties versus depth (mm), (c) δ^{13} C, (d) δ^{18} O, (e) Mg/Ca \times 10^{-3} , (f) Sr/Ca \times 10^{-3} and (g) Ba/Ca \times 10^{-3} records. Red lines indicate age model computed by Oxcal version 4.4 (Ramsey, 2008). Black dots and error bars represent 230 Th dating results and 2σ errors. Numbers indicate DO events from 8 to 14. (For interpretation of the references to color in this figure legend, the reader is referred to the Web version of this article.)

Table 1 $^{239} {\rm Th/U}$ dating results for stalagmite HJ1 from Huangjin Cave.

Sample	²³⁸ U (ppb)		²³² Th (ppt)		²³⁰ Th / ²³² Th (atomic x10 ⁻⁶)	ا (6-	δ^{234} U*		²³⁰ Th / ²³⁸ U		²³⁰ Th Age (ka BP)		²³⁰ Th Age (ka BP) (corrected)	(ka	$\delta^{234} U_{\text{initial}} **$	
						`	`		(6)		(======)			((======================================	
HJ-1-3	1767.5	0.2	2839.8	16.1	1863.2	10.7	756.66	0.41	0.1815	0.0002	11.73	0.01	11.71	0.02	782.07	0.42
HJ1-26	849.1	8.0	1913.7	38.4	4006.4	80.3	869.64	1.74	0.5476	90000	36.76	90.0	36.66	0.07	964.61	1.94
HJ1-47	1115.0	0.3	734.6	14.7	14272.1	285.2	903.00	1.09	0.5700	0.0007	37.63	90.0	37.62	90.0	1004.15	1.22
HJ1-62	1034.0	0.2	401.0	14.1	25368.6	894.7	960.39	1.53	0.5963	9000.0	38.28	90.0	38.28	90.0	1069.94	1.71
HJ1-73	1223.2	0.2	1603.0	16.3	7717.0	78.6	987.20	0.62	0.6131	9000.0	38.90	0.05	38.88	0.05	1101.69	0.71
HJ1-85	1014.6	0.2	3774.7	23.9	2698.9	17.3	929.00	0.59	0.6087	90000	39.98	0.05	39.93	90.0	1039.80	89.0
HJ1-100	1213.2	0.5	4227.7	26.0	2895.2	18.2	924.69	1.44	0.6116	0.0008	40.32	0.07	40.27	80.0	1035.97	1.63
HJ1-136	1148.4	0.4	6827.4	37.8	1715.8	9.7	912.93	1.25	0.6184	0.0007	41.15	0.07	41.06	80.0	1025.09	1.42
HJ1-152	784.2	0.1	3495.4	14.4	2378.7	10.0	911.41	0.46	0.6427	9000'0	43.12	0.05	43.05	90.0	1029.16	0.54
HJ1-162	620.9	0.1	521.6	14.3	12976.0	354.6	908.95	0.56	0.6608	0.0007	44.64	90.0	44.63	90.0	1030.94	0.65
HJ1-186	819.4	0.3	6.888	14.9	10242.9	172.5	901.24	1.36	0.6736	0.0009	45.91	80.0	45.89	80.0	1025.86	1.57
HJ1-186R	888.2	0.1	972.2	15.1	10164.8	158.4	900.73	0.65	0.6744	0.0007	45.99	90.0	45.98	90.0	1025.52	9.76
HJ1-220	836.8	0.1	2768.1	20.0	3466.4	25.3	927.32	0.65	0.6951	0.0007	46.88	90.0	46.83	0.07	1058.34	0.77
HJ1-225	1316.8	0.2	3196.1	21.4	4822.7	32.7	958.59	09.0	0.7096	0.0007	47.11	90.0	47.07	90.0	1094.78	0.71
HJ1-230	961.7	0.1	1571.9	16.4	7257.6	76.2	955.38	0.61	0.7191	0.0008	47.97	90.0	47.95	0.07	1093.81	0.72
HJ1-240	653.3	0.1	5952.9	33.4	1300.6	7.4	922.10	89.0	0.7184	0.0007	48.96	0.07	48.83	60.0	1058.34	0.83
HJ1-251	683.4	0.2	13375.5	9.69	601.6	3.2	886.71	1.17	0.7137	0.0008	49.72	80.0	49.44	0.16	1019.48	1.42
HJ1-271	787.1	0.1	2906.0	14.4	3157.3	15.9	824.36	0.44	0.7066	9000'0	51.26	90.0	51.21	0.07	952.53	0.54
HJ1-321	1014.8	0.2	4217.9	25.9	2801.0	17.4	743.83	0.58	0.7058	0.0007	54.25	0.07	54.19	80.0	866.73	0.71
HJ1-335	1105.9	0.1	14160.9	18.6	916.8	1.4	739.54	0.41	0.7116	9000'0	54.99	90.0	54.79	0.12	863.21	0.56
HJ1-335R	1255.7	0.1	5160.3	29.8	2853.2	16.7	748.66	0.27	0.7108	0.0007	54.54	0.07	54.47	80.0	873.07	0.37
HJ1-340	1055.9	0.1	5454.0	31.3	2261.8	13.2	736.36	0.41	0.7082	0.0007	54.79	0.07	54.71	0.08	859.29	0.51

U decay constants: $\lambda_{236} = 1.55125 \times 10^{-10} \, \mathrm{yr}^{-1}$ (Jaffey et al., 1971) and $\lambda_{234} = 2.82206 \times 10^{-6} \, \mathrm{yr}^{-1}$ (Cheng et al., 2013). Th decay constant: $\lambda_{230} = 9.1705 \times 10^{-6} \, \mathrm{yr}^{-1}$ (Cheng et al., 2013). *\$\delta_{234} \ \text{U}_{\text{inial}}\$ was calculated based on \$2.97 \text{h}\$ age (T), i.e. \$\delta_{234} \ \text{U}_{\text{inial}}\$ are a value of \$3.8.\$ The errors are arbitrarily assumed to be corrected \$2.30 \text{Th}\$ \text{Th}\$ ages assume the initial \$2.30 \text{Th}\$ at \$2.2) \times 10^{-6}\$. Those are the values for a material at secular equilibrium, with the bulk earth \$2.37 \text{Th}\$ /238 U value of 3.8. The errors are arbitrarily assumed to be \$8.00.\$\$\$\$**** Best of the searth of the search of the s

other within dating errors. However, compared with HJ1-355, the replicate of HJ1-355R is younger by 320 years, beyond dating errors. The 232 Th of HJ1-355 is three times higher than that of HJ1-355R, and therefore result of HJ1-355 could be easily affected by tailing effects during Th measurements and strongly influences the initial detrital 230 Th corrections. Considering the data quality, we use HJ1-355R to establish the age model. Therefore, 230 Th/U ages for stalagmite HJ1 are in stratigraphic order within 2σ uncertainties and show steady deposition at a rate of 0.017 mm/a. The age model for HJ1 was obtained using the Oxcal model version 4.4 under sequence "P" with Poisson parameter of 0.1 (Fig. 1b) (Ramsey, 2008). According to the age model, the sample HJ1 deposited during an interval from 55.2 to 36.5 ka BP (BP represents 1950 AD).

3.2. δ^{18} O and δ^{13} C sequences

Combined with chronology, we derive high-resolution stable isotope ($\delta^{18}O$ and $\delta^{13}C$) records with an average temporal resolution of ~30 years for stalagmite HJ1 (Fig. 1c and d). $\delta^{18}O$ values vary

from -10% to -6.9%, with an average of -8.7% and a range of 3.1%. δ^{13} C values range from -10.8% to -7.1%, with an average of -9.3% and an amplitude of 3.7%. Variations of the HJI δ^{18} O and δ^{13} C records are in-phased on the general trend, and the Pearson correlation in between is medium positive (r = 0.68, p < 0.01, n = 647; Table S1). Intense millennial-scale fluctuations are observed in both records, including seven negative excursions and two positive excursions. Within dating uncertainties, these negative/positive excursions correspond to DO events 8 to 14 and H events 4 and 5, respectively (Figs. 1 and 2).

Discrepancies exist in the δ^{18} O and δ^{13} C records in terms of the structures of these millennial-scale events. For instance, at the onsets of DO Interstadials, as constrained by dating results, negative excursions in δ^{13} C values are abrupt. After reaching the lowest values, δ^{13} C shifts towards positive values until the end of the Interstadial. In contrast, shifts in δ^{18} O record at the Interstadial onsets are relatively sluggish, and the δ^{18} O values stay at low-valued status for centuries before positive biases. Notably, negative peaks in δ^{13} C occur prior to those in δ^{18} O. These characteristics

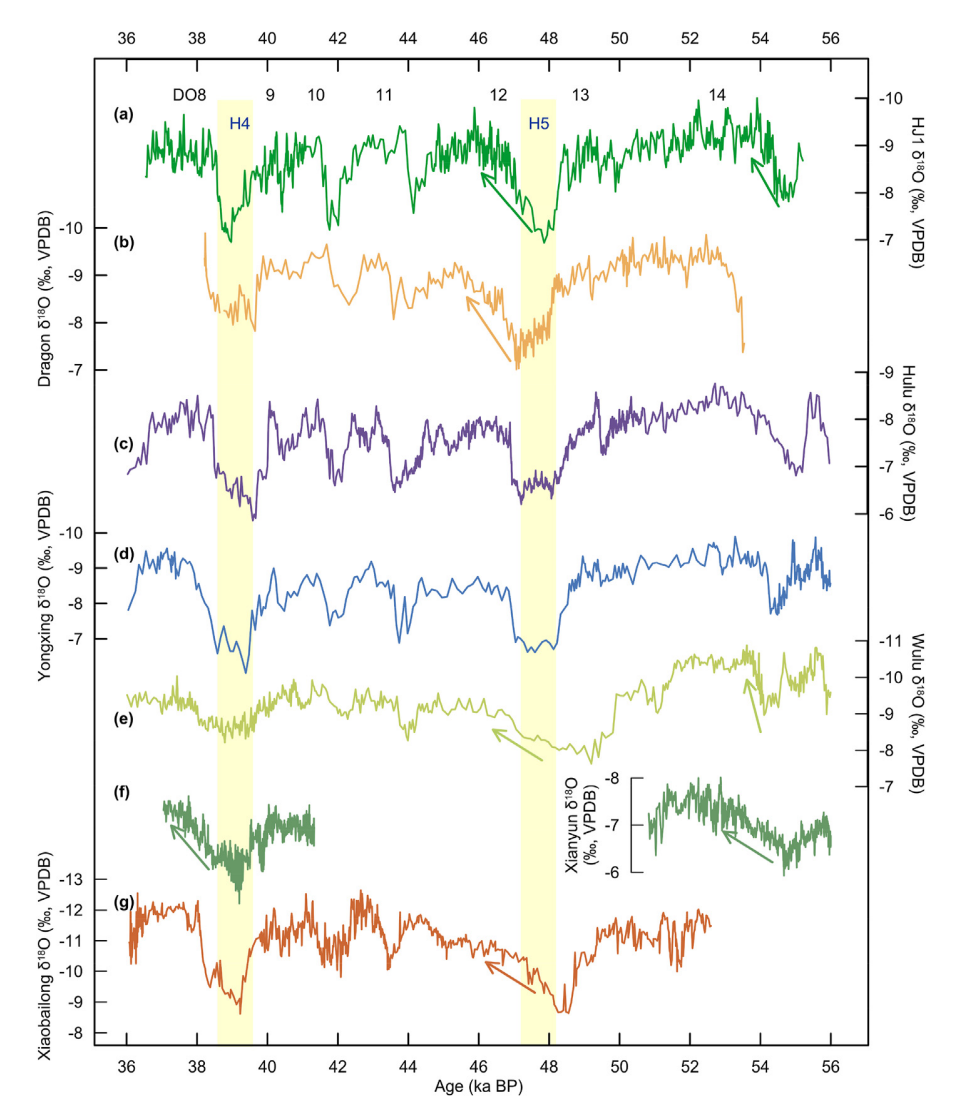


Fig. 2. Chinese δ^{18} O stalagmite records during the MIS3. δ^{18} O records are from (a) HJ1, (b) Dragon Cave (Dong et al., 2018), (c) Hulu Cave (Cheng et al., 2016; Liang et al., 2019), (d) Yongxing Cave (Chen et al., 2016), (e) Wulu Cave (Liu et al., 2018), (f) Xianyun Cave (Zhang et al., 2021a, 2021b) and (g) Xiaobailong Cave (Cai et al., 2006). Arrows indicate sluggish intensification of the EASM and yellow bars indicate Heinrich 4 and 5 events. (For interpretation of the references to color in this figure legend, the reader is referred to the Web version of this article.)

are more observable at two long-term DO onsets (Fig. 1c and d). These differences denote that the oxygen and carbon isotopic compositions in HJ1 are possibly controlled by different processes in climate and environmental changes.

Isotopic equilibrium is the prerequisite for the climatic application of stable isotopes in stalagmites. Two lines of evidence support the insignificant kinetic fractionation in HI1 sample. Firstly, Hendy test (Hendy, 1971) was performed on five individual growth laminae of sample HJ1 (Fig. S3). Results show that most δ^{18} O and δ^{13} C variations along the same layer range from 0.1% to 0.3% and an absence of relationship between $\delta^{18}O$ and $\delta^{13}C$, suggesting that the calcite deposited was close to equilibrium. Secondly, Dorale and Liu (2009) proposed the Replication test and in general, a strong similarity between different δ^{18} O records indicates small kinetic fractionation during the calcite deposition. Indeed, visual similarity is found among records from the monsoonal region of China (MRC) (Fig. 2). Comparison of our δ^{18} O record and other speleothem δ^{18} O curves from Dragon Cave (Dong et al., 2018), Hulu Cave (Cheng et al., 2016; Liang et al., 2019), Yongxing Cave (Chen et al., 2016), Wulu Cave (Liu et al., 2018) and Xiaobailong Cave (Cai et al., 2006) shows resemblant millennial-scale variabilities during the overlapped interval (Fig. 2). They all record H events as significant positive offsets by 1‰-3.3‰ and DO events as negative excursions larger than 1‰. In detail, we find that some of the Interstadial onsets in cave records are gradual, e.g. the DO12 in Huangjin, Dragon, Wulu and Xiaobailong caves, and the DO14 in Huangjin, Wulu and Xianyun caves (Fig. 2) (Cai et al., 2006; Dong et al., 2018; Liu et al., 2018; Zhang et al., 2021a, 2021b). Good replication between different cave records indicates minor disequilibrium in our δ^{18} O record. Under isotopic equilibrium conditions, HJ1 δ^{18} O record reliably reflect the δ^{18} O signals of meteoric precipitation and indicate a climatic origin (Dorale and Liu, 2009).

3.3. Trace metal compositions

Concentrations of Mg, Sr and Ba for stalagmite HJ1 are given as ratios with Ca. The Mg/Ca, Sr/Ca and Ba/Ca ratios range from 7.9×10^{-3} to 13.7×10^{-3} , 0.3×10^{-3} to 0.6×10^{-3} and 0.8×10^{-3} to 2.0×10^{-3} , respectively (Fig. 1e, f and g). Trace element ratios display weak correlations with each other, and they also display minor correlations with stable isotopic records (Table S1).

4. Discussions

4.1. Proxy interpretations for δ^{18} O and δ^{13} C

Studies have shown that speleothem and cave dripwater mainly inherits the δ^{18} O signals in precipitation, especially the wet-season recharge (Baker et al., 2019). In the MRC, the wet season corresponds to months from June to August and is dominantly under the control of the EASM when most of the total annual precipitation is received (Ding and Chan, 2005). The correlation between the amount-weighted annually-averaged precipitation (Yoshimura et al., 2008) and the annual summer rainfall ratio near our cave site reaches -0.42 (n = 38, p < 0.01) (Fig. S4a), indicating that δ^{18} O at Huangjin Cave was modulated by the EASM-related rainfall. A further comparison between the EASM index (Guo et al., 2004) and the amount-weighted $\delta^{18}O$ shows strong monsoon peak-to-peak correlated with negative δ^{18} O values and vice versa (Fig. S4c). Meanwhile, on the orbital and millennial timescales, stalagmite oxygen compositions are influenced by two processes: Wang-Cheng mechanism (changes in the fraction of monsoon rainfall in annual totals) and Yuan mechanism (changes in the amount of rainout between tropical sources and cave sites) (Liang et al., 2020). These two mechanisms together reflect the integrated rainfall from the moisture source to the cave, which could be regarded as the EASM intensity (Cheng et al., 2016; Liang et al., 2020). Therefore, both modern climatology and paleoclimatology focus on rainfall and wind, two key aspects of the monsoon. Apparently, Wang-Cheng mechanism is linked with rainfall changes. Yuan mechanism could be related with both rainfall and wind; because Rayleigh fractionation is related to the transportation of the air masses which is induced by the wind field in nature. Controlled by monsoonal climate, rainfall δ^{18} O at most sites in China displays similar seasonal variations, that is, higher δ^{18} O during boreal winter and spring, and lower values during boreal summer (Dayem et al., 2010). The consistency across the EASM region is also observable in the past. Indeed, as shown in Fig. 2, the strong resemblance of different δ^{18} O profiles in the East Asia indicates consistent response of monsoon intensity to climatic forcing and supports the idea of the continental-scale EASM circulation (He et al., 2021). Besides, changes in the NGRIP Ca²⁺ record shows comparable dust emissions to the intensity of the EASM, e.g. a rise of 200 ppb dust flux corresponding to 1% increase in δ^{18} O during Stadial 10 and 400 ppb to 2% during Stadial 9 (Fig. 3b and e). This is because wind gustiness is a primary driver of dust levels, and the major source for the Greenland dust lies in Asia which is strongly related with the monsoon circulation intensity (Sun, 2002; McGee et al., 2009). Therefore, speleothem δ^{18} O in Huangjin Cave, which mainly inherits summer rainfall isotopic compositions, could reflect the EASM intensity from both of the modern observation and the paleoclimate views.

In northern China, strong EASM intensity usually indicates high rainfall amount, with five reasons listed below. Firstly, meteorological observations find that modern precipitation δ^{18} O during the monsoon season in northern China has a high dependency on rainfall amount (Johnson and Ingram, 2004). Secondly, studies in Shihua Cave (Li et al., 2017), Wanxiang Cave (Zhang et al., 2008) and Wuya Cave (Tan, 2014) in northern China all confirm a robust antiphased relationship between speleothem $\delta^{18}O$ and rainfall amount. Thirdly, model simulations suggest that on the millennial timescale, Chinese stalagmite δ^{18} O could be used as a proxy for the EASM intensity and is consistent with precipitation amount in northern China (Liu et al., 2014; He et al., 2021). Fourthly, a high ratio of summer rainfall in annual totals near Huangjin Cave corresponds to high rainfall amount in a year (Fig. S4b). Furthermore, comparison of our δ^{18} O record with the reconstructed summer precipitation record from Jingyuan/Yuanbao loess profiles complements our argument, with lower δ¹⁸O values corresponding to higher precipitation amount and vice versa (Fig. 3e and f). Notably, the precipitation increases in loess at the onset of DO12 and DO14 are as gradual as that observed in our δ^{18} O record. Therefore, we suggest that HJ1 δ^{18} O record could not only reflect changes in the EASM intensity, but is more likely an indicator of precipitation variations in northern China.

We also notice that from the weakest to the strongest monsoonal statuses, onsets of DO12 and DO14 in different cave δ^{18} O records show different transitional characteristics (Fig. 2a–d). Although DO14 is incomplete in Dragon δ^{18} O record due to growth hiatus (Dong et al., 2018), DO12 in Dragon record is as sluggish as observed in our δ^{18} O record. Besides, Dragon record shows strong similarity with Huangjin in terms of the internal structures during the entire overlapped interval. In contrast, Hulu and Yongxing records display abrupt shifts at DO12 onset. These discrepancies between cave records could possibly be due to different contributions of Wang-Cheng mechanism and Yuan mechanism in different regions. Stalagmite δ^{18} O records in northern China (e.g. Huangjin and Dragon) to a large extent reflects rainfall amount (Wang-Cheng mechanism) (Li et al., 2017; Zhang et al., 2008; Tan, 2014), possibly by 25% or higher (Orland et al., 2015). Instead, stalagmite δ^{18} O

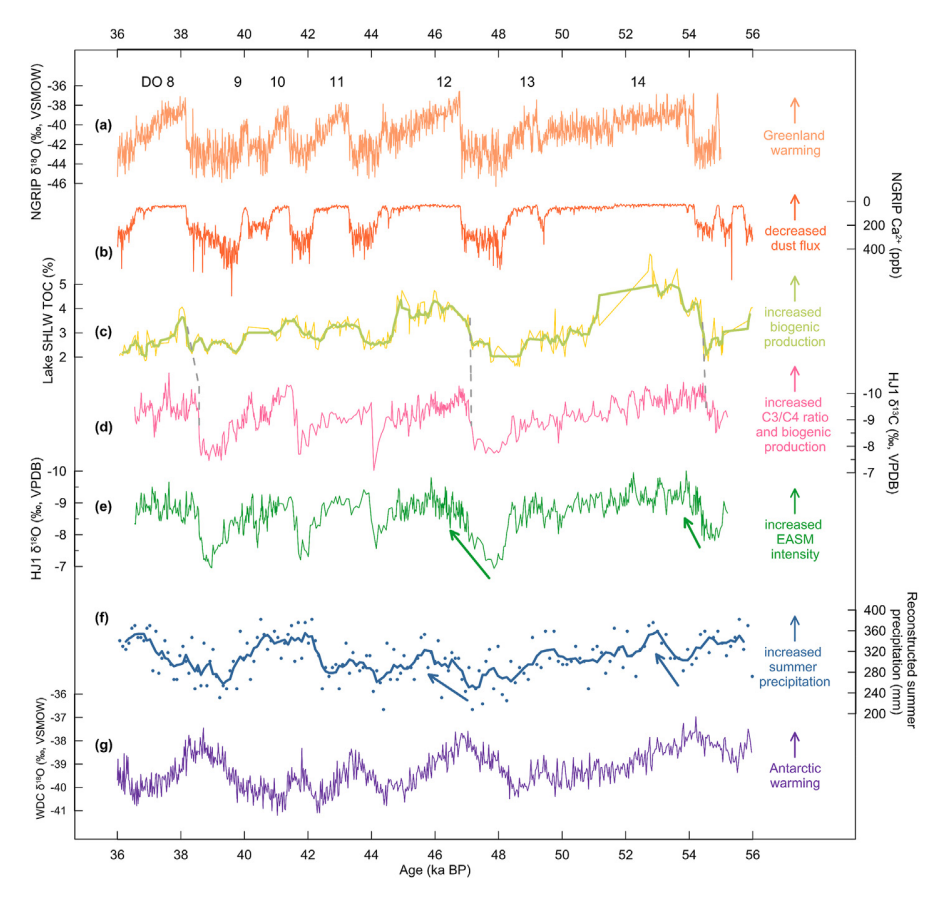


Fig. 3. Comparison of geological archives from around the globe: (a) δ^{18} O and (b) dust Ca²⁺ records of NGRIP ice core on the GICC05 chronology (North Greenland Ice Core Project Members, 2004; Svensson et al., 2008; Erhardt et al., 2019). (c) Total organic carbon (TOC) record of the Lake Sihailongwai (SHLW) (Mingram et al., 2018) and five-point running averages (thick line). (d) δ^{18} O and (e) δ^{13} C records of stalagmite HJ1. (f) Reconstructed summer precipitation record from organic δ^{13} C record of the Jingyuan and Yuanbao loess profiles (Rao et al., 2013) and five-point running averages (thick line). (g) δ^{18} O record from WDC ice core on the WD2014 chronology (WAIS Divide Project Members, 2015; Buizert et al., 2015). Dashed lines indicate abrupt shifts in cave and lake records. Slim arrows indicate gradual precipitation trend in cave and loess records.

records from Yangtze River Valley (YRV) (including Yongxing and Hulu) are more likely to reflect atmospheric circulation changes (Yuan mechanism), which are dominantly modulated by the El Niño Southern Oscillations (ENSO) (Tan, 2014; Wang et al., 2020). Both proxy records and cave monitoring data show that δ^{18} O in the YRV is not related with rainfall amount but the circulation index instead (Tan, 2014; Wang et al., 2020). Baker et al. (2015) also found large geographic variability of source and amount effects at different caves in China. Apparently, a better understanding of spatial pattern of isotopic signals in speleothem records calls for data which has better chronology and comparable resolution in the future

Speleothem δ^{13} C has complicated factors from external conditions (e.g. climate, vegetation, etc.) and during its deposition (e.g. cave ventilation, prior calcite precipitation (PCP), etc.), and thus it can provide important information on climatic and environmental changes (McDermott, 2004; Fairchild et al., 2006; Fohlmeister et al., 2020). In principle, carbon isotope compositions in stalagmites are dominantly sourced from the compositions of the soil CO₂, which is derived from biological processes (e.g. plant root respiration, oxidation of organic debris by microbial organisms) and vegetation type (C3 or C4 plants), namely biomass production or soil respiration (Cerling, 1984; Genty et al., 2003; McDermott, 2004; Fairchild et al., 2006; Lechleitner et al., 2021). Generally, under wet and warm climate conditions, increases in biological productivity due to exuberant vegetation and microbial activities would lead to higher

concentrations of 12 C-enriched soil CO₂ (Genty et al., 2003). The 12 C-enriched CO₂ is then transferred and deposited into secondary carbonate calcite, hence the low-valued calcite δ^{13} C during Interstadials. Along with external conditions, non-climate factors could also influence stalagmite δ^{13} C (McDermott, 2004; Fairchild et al., 2006). Modern observations and lab experiments show that decreased effective precipitation would extend the resistance time of the seepage water in the hostrock and slow down the drip rates, leading to significant increases in CO₂ degassing, PCP effects and δ^{13} C values in stalagmites, and vice versa (McDermott, 2004). Both climatic and non-climatic factors could possibly, to some extent, force δ^{13} C to change in the same direction.

Considering the isotopic equilibrium deposition and two lines of evidence below, we here suggest that HJ1 δ^{13} C is predominantly of biogenic origin. Firstly, the PCP effect in stalagmite HJ1 is falsified by the inconsistency of millennial-scale variations in three trace metal records (Fig. 1e, f and g), as well as the low correlation coefficients (<0.21) between trace metal ratios and δ^{18} O values (Table S1). As mentioned above, HJ1 δ^{18} O record is a good representation of the EASM intensity/rainfall amount and is featured with millennial-scale fluctuations. Besides, according to the PCP test proposed by Sinclair et al. (2012), the slope of the theoretical PCP gradient should be around 0.9. However, the slope of the trend line through the plot of ln (Mg/Ca) versus ln (Sr/Ca) is -0.5 in HJ1, indicating an absence of PCP control during calcite deposition. Secondly, the comparison between HJ1 δ^{13} C record and the total

organic carbon (TOC, an indicator of autochthonous biogenic production) record in Lake Sihailongwan (Mingram et al., 2018), northeastern China, further supports the biogenic interpretation. It is found that low HJ1 δ^{13} C values is consistent with high TOC production during Interstadials, and vice versa (Fig. 3c and d). Similar abrupt shifts are also observed in both records at the onsets of DO events (e.g. DO 8, 12 and 14). Meanwhile, from Stadials to Interstadials, the increase in C3/C4 ratio could cause decrease in calcite δ^{13} C values (Fleitmann et al., 2009; Zhao et al., 2017; Warken et al., 2019). This is due to the large difference between the typical δ¹³C values for secondary carbonates growing beneath C3 landscapes (-14% and -6%) and C4 systems (-6% to +2%) (McDermott, 2004; Fairchild et al., 2006). Lake Sihailongwan and Huangjin Cave locate close to each other (within 700 km), and nowadays both sites are dominantly covered with deciduous broad-leaved forest and coniferous forest (C3 plants). However, during the last glacial maximum and the early portion of the last deglaciation, both sites were primarily covered with steppe (C4 plants) (Li et al., 2019). Therefore, it is possible that under the same climate conditions (e.g. Interstadials and Stadials), vegetation type (C3 and C4 plant ratios) and biogenic production near Huangjin Cave would have similar revolutions as those near Lake Sihailongwan. In addition, during warm Interstadials, HJ1 δ^{13} C is lower because a higher proportion of biogenic CO2 dissolution in the seepage water, and this phenomenon has also been observed in other caves in the mid-latitude regions (Genty et al., 2003).

To sum up, HJ1 δ^{18} O is an indicator for the EASM precipitation intensity, while the δ^{13} C inherits the signatures of regional vegetation and biomass production. The in-phased variations of HJ1 δ^{18} O and δ^{13} C records are consistent with the seasonal climatic characteristics (synchronized temperature and rainfall changes) in northern China. Nevertheless, the discrepancies in both records

hint different responses to global changes, which will be discussed below.

4.2. Different response of calcite δ^{18} O and δ^{13} C to climate changes

As discussed above, HJ1 δ^{18} O and δ^{13} C records have in-phased variations on the millennial timescale. However, discrepancies exist in terms of the structure and onset timing of DO events in both records (Figs. 3 and 4). The onsets of DO events (especially DO12 and DO14) are much sluggish in δ^{18} O than in δ^{13} C, and the onsets in δ^{18} O lag or synchronize with those in δ^{13} C records (Fig. 4). Matching the midpoints of corresponding climate shifts is a traditional strategy for correlation/synchronization of proxy records (WAIS Divide Project Members, 2015; Buizert et al., 2015). Identification methods for each of the midpoints in DO transitions in our δ^{18} O and δ^{13} C records are the same as in Buizert et al. (2015). We manually determined the pre-event and post-event averages on the stalagmite chronology, as indicated by gray lines in Fig. 4a. The averaging time was set to around 200 years for Stadials and Interstadials according to the plateau part of the $\delta^{18}O$ and $\delta^{13}C$ profiles. After determining the pre- and post-event averages, we used linear interpolation of the time series to find the period at which the variable of interest completed 50% of the total transition (Fig. 4). We used the 50% marker as the midpoint of the transition, which was used for lead-lag comparison. We found that midpoints in δ^{13} C occur apparently advanced to those in $\delta^{18}O$ during two long DO events, DO12 and DO14, by 3.5 mm (around 200 years) and 7.5 mm (around 230 years), respectively (Fig. 4c and d, Table S2). As for other DO events, the onsets in two records are synchronous (Fig. 4a and b. Table S2). We also checked the lead-lag relationship in δ^{18} O and δ^{13} C records using the breakpoint method (Mudelsee, 2000, 2009) (Fig. S5). Although due to the low resolution (around 40–90

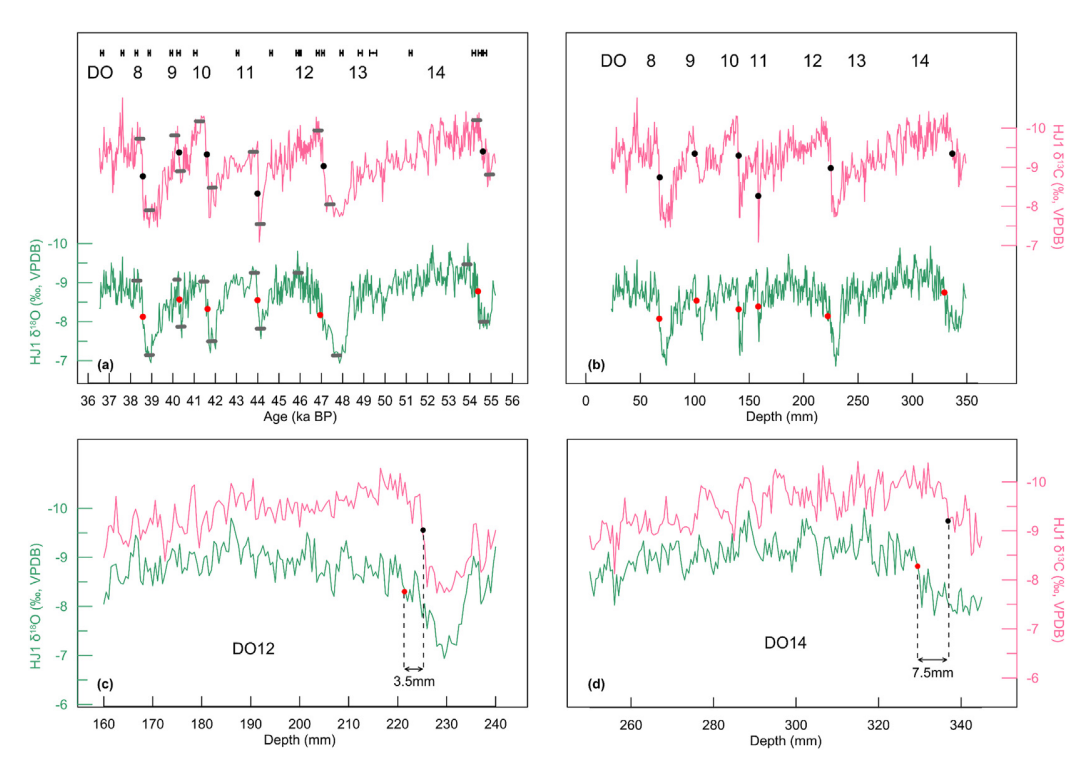


Fig. 4. Stable isotope records for stalagmite HJ1. (a) Records of δ^{18} O and δ^{13} C data versus age. (b) δ^{18} O and δ^{13} C data versus depth. (c) and (d) Enlarged sections of the comparison between δ^{18} O and δ^{13} C sequences on DO12 and DO14. Gray lines indicate pre-event and post-event averages, and black/red dots indicate midpoints in δ^{18} O and δ^{13} C records. Determination for midpoints is explained in section 4.2 with results shown in Table S2. (For interpretation of the references to color in this figure legend, the reader is referred to the Web version of this article.)

years) during the Stadials, breakpoints in only two DO events (DO8 and DO14) could be recognized, we still found synchronous DO8 onsets in both records and a $\delta^{13}\text{C-lead}$ in DO14 event by around 150 years. Therefore, both midpoint and breakpoint strategies have similar results on the lead-lag relationship in HJ1 records. These results could probably suggest that speleothem $\delta^{18}\text{O}$ (an indicator for the EASM intensity) and $\delta^{13}\text{C}$ (an indicator for vegetation type and biomass changes in northern China) have different responses to global climate changes.

We make further comparison with bipolar ice core records to understand the discrepancies of our δ^{18} O and δ^{13} C profiles (Fig. 5). Before that, we discuss the chronologies for different cores. During the studied time interval, the GICC05 chronology for NGRIP ice core in Greenland is based on annual layer counting (Andersen et al., 2006; Svensson et al., 2008). The GICC05 chronology could provide precise relative time (e.g. the duration for DO events), but the absolute age is less accurate due to the accumulated error of uncertain annual layers (Svensson et al., 2008). The age uncertainties for GICC05 from DO8 to DO14 range from 1449 to 2301 years (Buizert et al., 2015; Table S2). The WD2014 chronology for ice core WDC is established via synchronizing the midpoints in its methane record to those in the NGRIP $\delta^{18}O$ record and Hulu $\delta^{18}O$ record (Buizert et al., 2015). Then the ice age for WDC δ^{18} O record is derived by comparing the gas age using the gas age-ice age differences (Δ age, approximate to 351 \pm 73 years during MIS3) (Table S2) (Buizert et al., 2015). In the EASM-dominated region, chronologies for stalagmites are derived from ²³⁰Th/U dating which could provide independent age model and relatively small dating uncertainties. The average dating errors for Huangjin Cave is around ±70 years (Table 1 and Table S2). Obviously, stalagmites could provide better age constraints for millennial-scale events.

Comparison between HJ1 δ^{18} O and bipolar ice core records shows that despite the corresponding millennial-scale DO events, our δ^{18} O record shows better similarity with Antarctic temperature (Fig. 5). Within the combined dating error (<500 years) of WDC and HJ1, millennial-scale events in monsoon region and Antarctica are consistent, sluggish, "triangle" shaped and of nearly equivalent magnitudes. For instance, the sluggish shifts of calcite δ^{18} O around DO12 and 14 has gradual counterparts in WDC δ^{18} O (AIM12 and AIM14 events). These results support the view that on the millennial timescale, the EASM intensity is anti-phased correlated with

Antarctic temperature (Fig. 5b; Chen et al., 2016; Cheng et al., 2016; Rohling et al., 2009). The tight linkage between the EASM intensity and the Antarctic temperature could possibly be due to the thermal redistribution modulated by the AMOC (Stocker and Johnsen, 2003). The interhemispheric thermal contrast influences the EASM and the associated rainfall by the intensity of the crossequatorial airflow and the movement of the intertropical convergence zone (ITCZ) (Clemens et al., 1996; Chiang and Bitz, 2005; Schneider et al., 2014). As has been noted above, the crossequatorial airflow carries majority of the latent heat from the Indian Ocean, as a primary moisture source for summer precipitation at Huangjin site (Fig. S2). During DO Stadials, Antarctica warms up coherently with temperature increase over the SH, leading to a southward shift of the ITCZ, a diminishing cross-equatorial airflow, and finally the EASM weakening. Therefore, the EASM circulation is mutually affected by both hemispheres, but to a larger extent by the SH.

In contrast to the strong Antarctic imprints in speleothem $\delta^{18}O$ records, HJ1 δ^{13} C record mimics the characteristics in NGRIP δ^{18} O record on the millennial timescale, including "sawtooth" structure and abrupt shifts at DO onsets (Fig. 5a). Midpoints of DO onsets in HJ1 δ^{13} C record are averagely 400 years older than in NGRIP record, within the combined errors of layer counting uncertainties (1449-2301 years) and calcite $^{230}\text{Th/U}$ dating errors ($\pm 60 \text{ to} \pm 120 \text{ to}$ years) (Table 1). We also compare the durations of DO events in NGRIP δ^{18} O and HJ1 δ^{13} C record by calculating the length of midpoints and find slight duration discrepancies within 400 years. These results suggest that millennial-scale events are synchronous in NGRIP $\delta^{18}\text{O}$ and HJ1 $\delta^{13}\text{C}$ records, and low $\delta^{13}\text{C}$ values correspond to Greenland warming. In the Western Europe, calcite δ^{13} C record from Villars Cave (0°30′E, 45°18′N; Genty et al., 2003) in France also displays decreasing δ^{13} C values during Greenland warming, rapid δ^{13} C shifts at DO12 onset (Fig. S6b). Using multiple proxies and modelling, Lechleitner et al. (2021) confirmed that in the Western Europe, soil respired δ^{13} C (the source for speleothem δ^{13} C), was likely contributed from vegetation and biomass which was related to temperature changes. A possible mechanism that bridges the climate changes in northern high latitudes, western Europe, and northern China could be linked to the movements of the midlatitude westerly jet (Porter and An, 1995). An indicator of the jet wind path from Japan Sea sediments (Fig. S6c; Nagashima et al.,

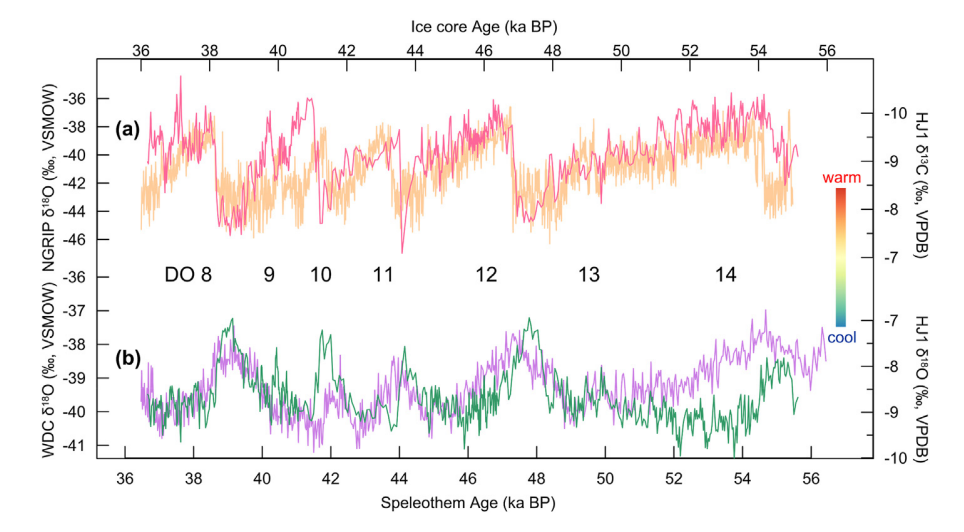


Fig. 5. Comparison between (a) NGRIP δ^{18} O record (North Greenland Ice Core Project Members, 2004) and stalagmite HJ1 δ^{13} C record, and (b) WDC δ^{18} O record (WAIS Divide Project Members, 2015) and HJ1 δ^{18} O record. Records are on independent chronologies, separately. The upper panel could be used as NH signals and the lower panel as SH signals. The colored bar on the left indicates the inverse bipolar temperature in Greenland and Antarctica.

2011) shows that the jet shifts between southern and northern positions are rapid during DO events. Meteorological studies also reveal that sea surface temperature changes in the North Atlantic, such as the Atlantic Multidecadal Oscillation, may modulate decadal-scale temperature changes in Europe and northeast Asia through the Silk Road pattern (Hong et al., 2017). The Silk Road pattern, which is an upper-tropospheric teleconnection pattern and spans across the Eurasian continent roughly along 40°N, is significantly related to the Asian westerly jet (Hong and Lu, 2016). Therefore, the harmony between Greenland temperature, calcite δ^{13} C and dust records at DO onsets (Figs. S6a-d) indicate rapid transitions of climatic signal through atmospheric processes. It is possible that northern high-latitude climate modulates hydrothermal conditions in northern China through westerly jet and/or Silk Road teleconnection, where Huangjin Cave locates, and subsequent changes in vegetation and biomass production are registered in speleothem δ^{13} C. Furthermore, in northern China, modern vegetation has a higher correlation with temperature than with rainfall; an increase in temperature could promote plant growth period in advance (starting from March to April, much earlier than the start of the EASM rainfall) and then extend the growth season (extending into November, much later than the end of the EASM rainfall) (Chen et al., 2000; Sun and Wang, 2015; Chu et al., 2019; Geng et al., 2019). Therefore, we suggest that climate parameters, especially temperature, plays a significant role in vegetation coverage and biomass in northern China, and finally the $\delta^{13}\text{C}$ values in stalagmite HJ1.

A lead of calcite δ^{13} C relative to δ^{18} O at onsets of DO12 and DO14 is identified, which could be caused by two factors (Fig. 4c and d). Firstly, on the seasonal timescale, the temperate vegetation in northern China begins growing from spring (March to April) (Chen et al., 2000; Wu et al., 2021; Zhang et al., 2021c), a few months earlier than the coming summer monsoon rainfall, but consistent with rapid seasonal warming (Fig. S1). Besides, the advance and extension of growth season are mainly related with increased spring temperature (Wu et al., 2021). Plants in northern China are more sensitive to temperature than precipitation and show no lagging time in response to spring warming (Sun and Wang, 2015: Chu et al., 2019; Geng et al., 2019; Zhang et al., 2021c), thus leading to an instant response of vegetation and soil δ^{13} C. The growth season of the temperate vegetation is apparently longer than the monsoon rainfall season (June-August, Fig. S1). Secondly, a lead of δ^{13} C to δ^{18} O at onsets of DO12 and 14 is caused by different climatic forcing on two proxies. For calcite δ^{18} O which documents the EASM intensity and monsoon rainfall in northern China, it is tightly coupled with the ITCZ and cross-equatorial airflow, modulated by the intensity of the AMOC and associated heat redistribution between hemispheres (oceanic processes). Whereas for calcite δ^{13} C, which is sourced from overlying vegetation and biomass, it is responsive to thermal conditions in northern China dominated by northern high-latitude climate through the westerly jet (atmospheric processes).

4.3. Bipolar lead-lag relationship based on stalagmite records

In section 4.2, we find that $\delta^{18}O$ and $\delta^{13}C$ records in stalagmite HJ1 have different preferences in response to the SH and NH climates. Here we further investigate the phase relationship of millennial-scale events between the SH and NH from one stalagmite, which could avoid the chronological biases in different cores. Based on the strong similarity and dynamic linkages of millennial-scale events between Chinese cave $\delta^{18}O$ and Antarctic temperature records induced from our and previous studies (e.g. Chen et al., 2016; Cheng et al., 2016), we suggest that during the transitions from Stadials to Interstadials, the initial change points in

speleothem δ^{18} O record are synchronous with breakpoints in the AIM events. For DO14, the midpoint in δ^{13} C record takes place in advance of δ^{18} O record, indicating that onsets of DO events could possibly occur prior to the EASM and the Antarctic climate changes. We roughly calculated the initial change point in δ^{18} O record (which represents the start of monsoon recovery) for DO14 and found that it was older than δ^{18} O midpoint by ~110 years (Fig. 6a). Now that the δ^{13} C midpoint occur prior to δ^{18} O record by ~230 years (Table S2), it should take place ahead of the breakpoints of AIM events by ~120 years (Fig. 6a).

The ~120-year NH lead at DO14 onset in our study supports the work by WAIS Divide Project Members (2015) which utilized the methane-synchronization method and found a NH lead by 218 \pm 92 years. Our results also support their idea that triggers for DO onsets possibly reside in the northern high-latitude regions and the ocean conveyor plays an important role of transmission (WAIS Divide Project Members, 2015; Pedro et al., 2018). Upon the rapid sea ice melting in the Nordic Sea (Wary et al., 2016), the abrupt retreat of thick ice shelves near Greenland (Boers et al., 2018) or the disturbance of the salt oscillator (Peltier and Vettoretti, 2014), etc., whichever should be the causal agents for DO events, the Greenland temperature shifts from cold conditions into warm conditions. Temperature in the NH is then warmed up, leading to warming in northern China, flourishing vegetation, and increasing biomass production and soil respiration. Compared with the fast transfer of atmospheric processes within several decades, the oceanic processes require hundreds to thousands of years to complete (Liu and Alexander, 2007; Pedro et al., 2018), causing the delayed heat redistribution between hemispheres. Accompanied with AMOC changes are the movements of the ITCZ and the intensity of the cross-equatorial air mass (Chiang and Bitz, 2005). Meanwhile, the massive thermal capacity of the ocean also forces slow surface temperature cooling in both the Southern Ocean and the Antarctica (Blunier and Brook, 2001; Stocker and Johnsen, 2003; Markle et al., 2017), which possibly contributes to the sluggish intensification of the EASM (Cai et al., 2006; Chen et al., 2016).

Furthermore, short-term DO events (e.g. DO8) in δ^{13} C and δ^{18} O records are synchronous (Table S2 and Fig. S5). In this case, the initial change points in HJ1 δ^{18} O record and the breakpoints in AIM events occur ahead of the midpoints in NGRIP by ~150 years (Fig. 6b). Actually, Raisbeck et al. (2017) found that in AIM8 and AIM10, the main δ^{18} O decrease in Antarctica occurred ~200 years before the Greenland temperature increase. Our results provide support to their estimations and their idea that "the lead/lag of Greenland vs. Antarctica may be different from one event to another" (Raisbeck et al., 2017). Under conditions of the Antarctic lead, the Southern Ocean could be the generator for millennialscale events and the AMOC recovery. During the last deglaciation, rapid resumption of the AMOC and the onset of Bølling-Allerød is initially triggered by the Meltwater Pulse 1A which is contributed from the SH (Weaver et al., 2003). Studies suggest that Antarctic meltwater discharge could lead to cooling in the Southern Ocean but warming in the North Atlantic and the initial EASM strengthening (Swingedouw et al., 2008; Zhang et al., 2016), Meanwhile, a leakage of the Agulhas currents could also assist the recovery of the AMOC by providing buoyancy compensation and triggering increased convective activity in the North Atlantic, thereby leading to the onsets of Interstadials (Beal et al., 2011).

According to the phase relationship between $\delta^{13}C$ and $\delta^{18}O$ from stalagmite HJ1, we find that the onsets of abrupt climate changes could be triggered either in the NH or the SH. This is somehow consistent with Cheng et al. (2020)'s results on Younger Dryas (YD) event. They found that YD started from the North Atlantic and was advanced of the Antarctica by around 100 years; however, the ending of the YD came first in the Antarctica and led climate

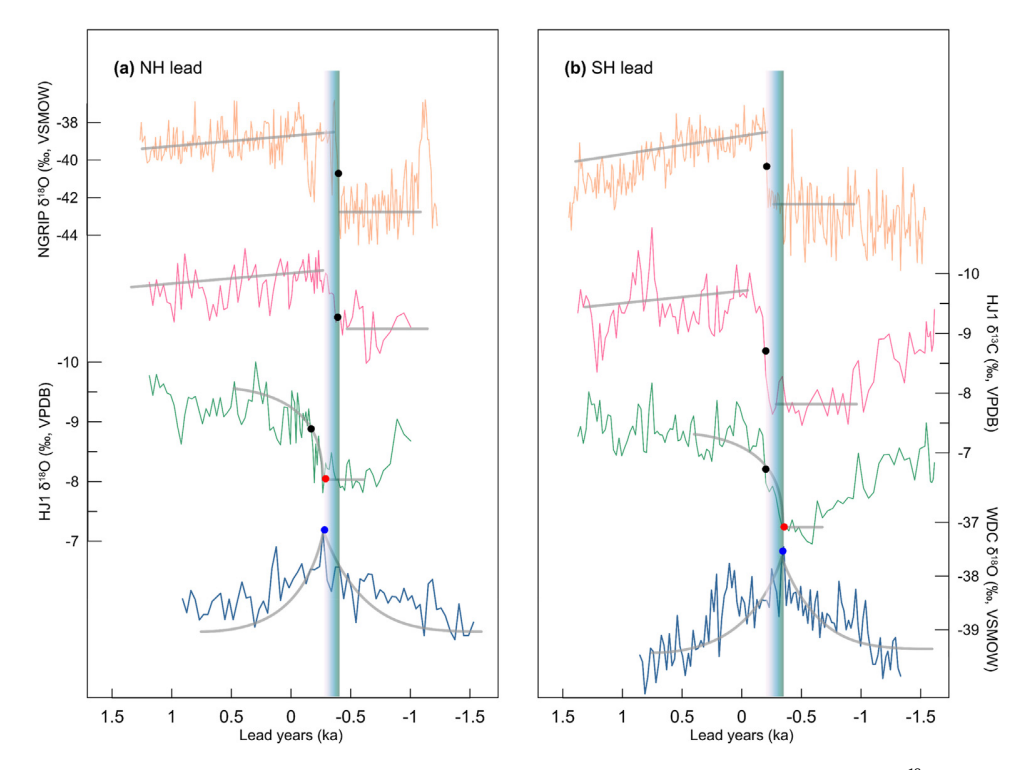


Fig. 6. Illustration of the lead-lag mode for bipolar see-saw, using the example of DO14 (a) and DO8 (b). From top to bottom are: NGRIP δ^{18} O record (North Greenland Ice Core Project Members, 2004), HJ1 δ^{13} C record, HJ1 δ^{18} O record and WDC δ^{18} O record (WAIS Divide Project Members, 2015). Gray curves indicate trends in each record. Black points indicate midpoints in NGRIP δ^{18} O and HJ1 δ^{13} C record, red ones indicate initial change points in HJ1 δ^{18} O record, and blue ones indicate breakpoints in WDC δ^{18} O record. Colored vertical bars are used to indicate the time intervals between the midpoints of HJ1 δ^{13} C and the initial points of HJ1 δ^{18} O record. (For interpretation of the references to color in this figure legend, the reader is referred to the Web version of this article.)

changes in the NH by ~200 years (Cheng et al., 2020). Recently, Cheng et al. (2021) also found that hundreds of years prior to the H4 termination, the Amazon River discharge decreased and the SH westerly wind and subtropical front shifted poleward, suggesting that the initial trigger for H4 might reside in SH. We admit that the comparison between HJ1 proxies might be somewhat limited by age uncertainties. For example, uncertainties for the lead-lag durations (hundreds of years) between HJ1 δ^{13} C and δ^{18} O records depend on the derived ²³⁰Th/U dating and the established chronology. And a closer inspection shows better temporal resolution for HI1 during Interstadials than during Stadials, leading to ambiguous structures of our records during Stadials. These shortages hamper the determination for the initial change points of DO events in records. Anyway, this paper is an attempt for understanding the interhemispheric lead-lag relationship from one speleothem, and we expect a more precise phase relationship for "bipolar see-saw" from cave work in the future, with better age constraints and temporal resolutions.

5. Conclusions

A new $^{230}\text{Th/U}$ dated, ~30-year-resolution stalagmite record from Huangjin Cave, Hebei Province, provides us with new insights into millennial-scale paleoclimate variations during last glacial period from 55.2 to 36.5 ka BP. The HJ1 $\delta^{18}\text{O}$ and $\delta^{13}\text{C}$ records display in-phased variations on the general trend and large-amplitude and millennial-scale fluctuations, corresponding to DO cycles from 8 to 14 and two H events. However, discrepancies exist in terms of event structures in two proxy records; that is, sluggish shifts and trapezoid shape in $\delta^{18}\text{O}$ record whereas rapid offsets and right-triangle shape in $\delta^{13}\text{C}$ record. Besides, negative shifts in $\delta^{13}\text{C}$

occur prior to those in δ^{18} O profiles, particularly in the long-term DO events. These differences denote that the oxygen and carbon isotopic compositions in HI1 are possibly controlled by different processes in climate and environmental changes. Further comparison with other geological archives indicates a strong resemblance (abrupt shifts and sawtooth pattern) of HJ1 δ^{13} C to the NGRIP δ^{18} O and SHLW TOC records. These findings suggest that northern highlatitude climate could modulate temperature changes in northern China through the westerly jet, affecting vegetation and biomass production and thereby the carbon compositions in HJ1. Otherwise, HJ1 δ^{18} O displays a better similarity with WDC δ^{18} O and JY/YB precipitation records, indicating that the monsoon circulation and related rainfall is more likely linked with the SH through the movement of the ITCZ and the intensity of the cross-equatorial airflows. In addition, the lead-lag phase relationship between the SH and NH is discussed. Midpoints of DO14 onsets in δ^{13} C record occur ~230 years prior to that in δ^{18} O records, leading to a ~120year lead of the NH relative to the SH. This result indicates that onsets of some DO events could possibly occur prior to the EASM intensification and Antarctic cooling. However, midpoints and breakpoints of DO8 event is coeval in δ^{13} C and δ^{18} O records. In this case, the breakpoints of AIM events take place ahead of DO onsets by ~150 years. These results suggest that "bipolar see-saw" is most likely controlled by the classical ocean circulation mechanism, and the Greenland vs. Antarctica relationship is dependent on the trigger source for the AMOC.

Author contributions

Yijia Liang: Investigation, Data curation, Writing - Original Draft. **Kan Zhao**: Resources, Conceptualization, Funding

acquisition, Writing- Reviewing and Editing, Project administration. **Yongjin Wang**: Supervision, Writing- Reviewing and Editing, Funding acquisition. **R. Lawrence Edwards**: Funding acquisition, Writing- Reviewing and Editing. **Hai Cheng**: Data curation. **Qingfeng Shao**: Data curation. **Shitao Chen:** Funding acquisition. **Jinyu Wang**: Data curation. **Junji Zhu**: Data curation.

Declaration of competing interest

The authors declare that they have no known competing financial interests or personal relationships that could have appeared to influence the work reported in this paper.

Acknowledgement

This work was supported by National Natural Science Foundation of China (awards 42071105, 41931178, 42072207), the U.S. Nature Science Foundation (award 1702816), and the 111 Program of China (award D19002).

Appendix A. Supplementary data

Supplementary data to this article can be found online at https://doi.org/10.1016/j.guascirev.2021.107305.

References

- Andersen, K.K., Svensson, A., Johnsen, S.J., Rasmussen, S.O., Bigler, M., Rothlisberger, R., Ruth, U., Siggaard-Andersen, M.-L., Peder Steffensen, J., Dahl-Jensen, D., Vinther, B.M., Clausen, H.B., 2006. The Greenland Ice Core Chronology 2005, 15–42 ka. Part 1: constructing the time scale. Quat. Sci. Rev. 25, 3246–3257.
- Baker, A., Ito, E., Smart, P.L., Mcewan, R.F., 1997. Elevated and variable values of δ^{13} C in speleothems in a British cave system. Chem. Geol. 136, 263–270.
- Baker, A.J., Sodemann, H., Baldini, J.U.L., Breitenbach, S.F.M., Johnson, K.R., van Hunen, J., Zhang, P., 2015. Seasonality of westerly moisture transport in the East Asian summer monsoon and its implications for interpreting precipitation δ¹⁸O. J. Geophys. Res. Atm. 120, 5850–5862.
- Baker, A., Hartmann, A., Duan, W., Hankin, S., Comas-Bru, L., Cuthbert, M., Treble, P., Banner, J., Genty, D., Baldini, L., Bartolomé, M., Moreno, A., Pérez-Mejías, C., Werner, M., 2019. Global analysis reveals climatic controls on the oxygen isotope composition of cave drip water. Nat. Commun. 10, 2984. https://doi:10. 1038/s41467-019-11027-w.
- Bar-Matthews, M., Ayalon, A., Kaufman, A., 1997. Late quaternary paleoclimate in the eastern mediterranean region from stable isotope analysis of speleothems at Soreq cave, Israel. Quat. Res. 47, 155–168.
- Beal, L.M., De Ruijter, W.P.M., Biastoch, A., Zahn, R., 2011. On the role of the Agulhas system in ocean circulation and climate. Nature 472, 429–436.
- Blunier, T., Chappellaz, J., Schwander, J., Dällenbach, A., Stauffer, B., Stocker, T.F., Raynaud, D., Jouzel, J., Clausen, H.B., Hammer, C.U., Johnsen, S.J., 1998. Asynchrony of Antarctic and Greenland climate change during the la st glacial period. Nature 394, 739—743.
- Blunier, T., Brook, E.J., 2001. Timing of Millennial-scale climate change in Antarctica and Greenland during the last glacial period. Science 291, 109—112.
- Boers, N., Ghil, M., Rousseau, D., 2018. Ocean circulation, ice shelf, and sea ice interactions explain Dansgaard—Oeschger cycles. Proc. Natl. Acad. Sci. Unit. States Am. 115, E11005—E11014.
- Broecker, W.S., 1998. Paleocean circulation during the last deglaciation: a bipolar seesaw? Paleoceanography 13 (2), 119–121.
- Buizert, C., Cuffey, K., Severinghaus, J., Baggenstos, D., Fudge, T.J., Steig, E., Markle, B.R., Winstrup, M., Rhodes, R., Brook, E., Sowers, T., Clow, G., Cheng, H., Edwards, R., Sigl, M., McConnell, J., Taylor, K., 2015. The WAIS Divide deep ice core WD2014 chronology Part 1: methane synchronization (68–31 ka BP) and the gas age—ice age difference. Clim. Past 11, 153–173.
- Buizert, C., Schmittner, A., 2015. Southern Ocean control of glacial AMOC stability and Dansgaard-Oeschger interstadial duration. Paleoceanography 30, 1595–1612.
- Buizert, C., Sigl, M., Severi, M., Markle, B.R., Wettstein, J., McConnell, J., Pedro, J., Sodemann, H., Goto-Azuma, K., Kawamura, K., Fujita, S., Motoyama, H., Hirabayashi, M., Uemura, R., Stenni, B., Parrenin, F., He, F., Fudge, T.J., Steig, E., 2018. Abrupt ice-age shifts in southern westerly winds and Antarctic climate forced from the north. Nature 563, 681–685.
- Cai, Y., An, Z., Cheng, H., Edwards, R., Kelly, M.J., Liu, W., Wang, X., Shen, C., 2006. High-resolution absolute-dated Indian Monsoon record between 53 and 36 ka from Xiaobailong Cave, southwestern China. Geology 34, 621–624.
- Cerling, T., 1984. The stable isotopic composition of modern soil carbonate and its

- relationship to climate. Earth Planet Sci. Lett. 71, 229-240.
- Chen, S., Wang, Y., Cheng, H., Edwards, R., Wang, X., Kong, X., Liu, D., 2016. Strong coupling of Asian Monsoon and Antarctic climates on sub-orbital timescales. Sci. Rep. 6, 32995. https://doi:10.1038/srep32995.
- Chen, X., Tan, Z., Schwartz, M., Xu, C.X., 2000. Determining the growing season of land vegetation on the basis of plant phenology and satellite data in Northern China. Int. J. Biometeorol. 44, 97–101.
- Cheng, H., Edwards, R., Hoff, J.A., Gallup, C., Richards, D., Asmerom, Y., 2000. The half-lives of uranium-234 and thorium-230. Chem. Geol. 169, 17–33. Cheng, H., Edwards, R.L., Shen, C., Polyak, V.J., Asmerom, Y., Woodhead, J.,
- Cheng, H., Edwards, R.L., Shen, C., Polyak, V.J., Asmerom, Y., Woodhead, J., Hellstrom, J., Wang, Y., Kong, X., Spötl, C., 2013. Improvements in ²³⁰Th dating, ²³⁰Th and ²³⁴U half-life values, and U-Th isotopic measurements by multicollector inductively coupled plasma mass spectrometry. Earth Planet. Sci. Lett. 371, 82–91.
- Cheng, H., Edwards, R.L., Sinha, A., Spötl, C., Yi, L., Chen, S., Kelly, M., Kathayat, G., Wang, X., Li, X., Kong, X., Wang, Y., Ning, Y., Zhang, H., 2016. The Asian monsoon over the past 640,000 years and ice age terminations. Nature 534, 640–646.
- Cheng, H., Zhang, H., Spötl, C., Baker, J.L., Sinha, A., Li, H., Bartolomé, M., Moreno, A., Kathayat, G., Zhao, J., Dong, X., Li, Y., Ning, Y., Jia, X., Zong, B., Brahim, Y.A., Pérez-Mejías, C., Cai, Y., Novello, V., Cruz, F., Severinghaus, J., An, Z., Edwards, R., 2020. Timing and structure of the Younger Dryas event and its underlying climate dynamics. Proc. Natl. Acad. Sci. Unit. States Am. 117, 23408–23417.
- Cheng, H., Xu, Y., Dong, X., Zhao, J., Li, H., Baker, J., Sinha, A., Spötl, C., Zhang, H., Du, W., Zong, B., Jia, X., Kathayat, G., Liu, D., Cai, Y., Wang, X., Strikis, N.M., Cruz, F.W., Auler, A.S., Gupta, A.K., Singh, R.K., Jaglan, S., Dutt, S., Liu, Z., Edwards, R.L., 2021. Onset and termination of Heinrich Stadial 4 and the underlying climate dynamics. Commun. Earth Environ. 2, 230.
- Chiang, J.C.H., Bitz, C.M., 2005. Influence of high latitude ice cover on the marine Intertropical Convergence Zone. Clim. Dynam. 25, 477–496.
- Chu, H., Venevsky, S., Wu, C., Wang, M., 2019. NDVI-based vegetation dynamics and its response to climate changes at Amur-Heilongjiang River Basin from 1982 to 2015. Sci. Total Environ. 650, 2051–2062.
- Clemens, S., Murray, D., Prell, W., 1996. Nonstationary phase of the plio-pleistocene Asian monsoon. Science 274, 943–948.
- Dayem, K.E., Molnar, P., Battisti, D.S., Roe, G.H., 2010. Lessons learned from oxygen isotopes in modern precipitation applied to interpretation of speleothem records of paleoclimate from eastern Asia. Earth Planet Sci. Lett. 295, 219–230.
- Ding, Y.H., Chan, J.C.L., 2005. The East Asian summer monsoon: an overview. Meteorol. Atmos. Phys. 89, 117–142.
- Dong, J., Shen, C., Kong, X., Wang, Y., Duan, F., 2018. Asian monsoon dynamics at Dansgaard/Oeschger events 14—8 and Heinrich events 5—4 in northern China. Quat. Geochronol. 47, 72—80.
- Dorale, J.A., González, L.A., Reagan, M.K., et al., 1992. A high-resolution record of holocene climate change in speleothem calcite from cold water cave, northeast lowa. Science 258, 1626—1630.
- Dorale, J.A., Liu, Z., 2009. Limitations of Hendy test criteria in judging the paleoclimatic suitability of speleothems and the need for replication. J. Cave Karst Stud. 71, 73–80.
- Edwards, R.L., Chen, J., Wasserburg, G., 1987. ²³⁸U-²³⁴U-²³⁰Th-²³²Th systematics and the precise measurement of time over the past 500,000 years. Earth Planet Sci. Lett. 81, 175–192.
- Edwards, R.L., Gallup, C.D., Cheng, H., 2003. Uranium-series dating of marine and lacustrine carbonates. Rev. Mineral. Geochem. 52, 363–405.
- EPICA Community Members, 2006. One-to-one coupling of glacial climate variability in Greenland and Antarctica. Nature 7116, 195–198.
- Erhardt, T., Capron, E., Rasmussen, S., Schüpbach, S., Bigler, M., Adolphi, F., Fischer, H., 2019. Decadal-scale progression of the onset of Dansgaard—Oeschger warming events. Clim. Past 15, 811–825.
- Fairchild, I., Smith, C., Baker, A., Fuller, L., Spötl, C., Mattey, D., McDermott, F., 2006. Modification and preservation of environmental signals in speleothems. Earth Sci. Rev. 75, 105–153.
- Fleitmann, D., Cheng, H., Badertscher, S., Edwards, R.L., Mudelsee, M., Göktürk, O.M., Fankhauser, A., Pickering, R., Raible, C.C., Matter, A., Kramers, J., Tüysüz, O., 2009. Timing and climatic expression of Dansgaard-Oeschger events in stalagmites from Sofular Cave, Turkey. Geophys. Res. Lett. 34, L19707. https://doi: 10.1029/2009GL040050.
- Fohlmeister, J., Voarintsoa, N.R., Lechleitner, F., Boyd, M., Brandtstatter, S., Jacobson, M., Oster, J., 2020. Main controls on the stable carbon isotope composition of speleothems. Geochem. Cosmochim. Acta 279, 67–87.
- Frappier, A., Sahagian, D., González, L.A., Carpenter, S.J., 2002. El Niño events recorded by stalagmite carbon isotopes. Science 298, 565, 565.
- Geng, R., Zhao, Y., Cui, Q., Qin, F., 2019. Representation of modern pollen assemblages with respect to vegetation and climate in Northeast China. Quat. Int. 532, 126–137.
- Genty, D., Blamart, D., Ouahdi, R., Gilmour, M., Baker, A., Jouzel, J., Van-Exter, S., 2003. Precise dating of Dansgaard—Oeschger climate oscillations in western Europe from stalagmite data. Nature 421, 833–837.
- Guo, Q., Cai, J., Shao, X., Sha, W., 2004. Studies on the variations of East Asian summer monsoon during AD 1873-2000. Chin. J. Atmos. Sci. 28, 206–216.
- He, C., Liu, Z., Otto-Bliesner, B., Brady, E., Zhu, C., Tomas, R., Clark, P., Zhu, J., Jahn, A., Gu, S., Zhang, J., Nusbaumer, J., Noone, D., Cheng, H., Wang, Y., Yan, M., Bao, Y., 2021. Hydroclimate footprint of pan-Asian monsoon water isotope during the last deglaciation. Sci. Adv. 7, eabe2611.
- Hendy, C.H., 1971. The isotopic geochemistry of speleothems-I. The calculation of the effects of different modes of formation on the isotopic composition of

- speleothems and their applicability as palaeoclimatic indicators. Geochem. Cosmochim. Acta 35, 801–824.
- Hong, X., Lu, R., 2016. The meridional displacement of the summer Asian jet, Silk Road pattern, and tropical SST anomalies. J. Clim. 29, 3753-3766.
- Hong, X., Lu, R., Li, S., 2017. Amplified summer warming in Europe-West Asia and northeast Asia after the mid-1990s, Environ, Res. Lett. 12, 094007.
- Jaffey, A.H., Flynn, K.F., Glendenin, L.E., Bentley, W.C., Essling, A.M., 1971. Precision measurement of half-lives and specific activities of ²³⁵U and ²³⁸U. Phys. Rev. C 4, 1889-1906.
- Johnson, K.R., Ingram, B.L., 2004. Spatial and temporal variability in the stable isotope systematics of modern precipitation in China: implications for paleoclimate reconstructions. Earth Planet Sci. Lett. 220, 365–377.
- Knutti, R., Flückiger, J., Stocker, T., Timmermann, A., 2004. Strong hemispheric coupling of glacial climate through freshwater discharge and ocean circulation. Nature 430, 851-856.
- Landais, A., Masson-Delmotte, V., Stenni, B., Selmo, E., Roche, D.M., Jouzel, J., Lambert, F., Guillevic, M., Bazin, L., Arzel, O., Vinther, B., Gkinnis, V., Popp, T., 2015. A review of the bipolar see-saw from synchronized and high resolution ice core water stable isotope records from Greenland and East Antarctica. Quat. Sci. Rev. 114, 18-32.
- Lechleitner, F.A., Day, C.C., Kost, O., Wilhelm, M., Haghipour, N., Henderson, G.M. Stoll, H.M., 2021. Stalagmite carbon isotopes suggest deglacial increase in soil respiration in Western Europe driven by temperature change. Clim. Past 17, 1903-1918
- Li, X., Cheng, H., Tan, L., Ban, F., Sinha, A., Duan, W., Li, H., Zhang, H., Ning, Y., Kathayat, G., Edwards, R., 2017. The East Asian summer monsoon variability over the last 145 years inferred from the Shihua Cave record. North China, Sci. Rep. 7, 7078.
- Li, O., Wu, H., Yu, Y., Sun, A., Luo, Y., 2019. Large-scale vegetation history in China and its response to climate change since the Last Glacial Maximum, Quat, Int. 500, 108-119.
- Liang, Y., Wang, Y., Wang, Q., Wu, J., Shao, Q., Zhang, Z., Yang, S., Kong, X., Edwards, R., 2019. East Asian summer monsoon climates and cave hydrological cycles over Dansgaard-Oeschger events 14 to 11 revealed by a new stalagmite record from Hulu Cave. Quat. Res. 92, 725-737.
- Liang, Y., Zhao, K., Edwards, R., Wang, Y., Shao, Q., Zhang, Z., Zhao, B., Wang, Q., Cheng, H., Kong, X., 2020. East Asian monsoon changes early in the last deglaciation and insights into the interpretation of oxygen isotope changes in the Chinese stalagmite record. Quat. Sci. Rev. 250, 106699.
- Liu, D., Wang, Y., Cheng, H., Edwards, R., Kong, X., Chen, S., Liu, S., 2018. Contrasting patterns in abrupt Asian summer monsoon changes in the last glacial period and the holocene. Paleoceanogr. Paleoclimatol. 33, 214–226.
- Liu, Z., Alexander, M., 2007. Atmospheric bridge, oceanic tunnel, and global climatic teleconnections. Rev. Geophys. 45, RG2005.
- Liu, Z., Wen, X., Brady, E., Otto-Bliesner, B., Yu, G., Lu, H., Cheng, H., Wang, Y., Zheng, W., Ding, Y., Edwards, R., Cheng, J., Liu, W., Yang, H., 2014. Chinese cave records and the east Asia summer monsoon. Quat. Sci. Rev. 83, 115-128.
- Lund, D., Hertzberg, J., Lacerra, M., 2019. Carbon isotope minima in the South Atlantic during the last deglaciation: evaluating the influence of air-sea gas exchange. Environ. Res. Lett. 14, 055004.
- Markle, B.R., Steig, E.J., Buizert, C., Schoenemann, S.W., Bitz, C.M., Fudge, T.J., Pedro, J.B., Ding, Q., Jones, T.R., White, J.W.C., Sowers, T., 2017. Global atmospheric teleconnections during dansgaard-oeschger events. Nat. Geosci. 10,
- McDermott, F., 2004. Palaeo-climate reconstruction from stable isotope variations in speleothems: a review. Quat. Sci. Rev. 23, 901-918.
- McGee, D., Broecker, W., Winckler, G., 2009. Gustiness: the driver of glacial dustiness? Quat. Sci. Rev. 29, 2340-2350.
- Mingram, J., Stebich, M., Schettler, G., Hu, Y., Rioual, P., Nowaczyk, N., Dulski, P., You, H., Opitz, S., Liu, Q., Liu, J., 2018. Millennial-scale East Asian monsoon variability of the last glacial deduced from annually laminated sediments from Lake Sihailongwan, N.E. China. Quat. Sci. Rev. 201, 57-76.
- Mudelsee, M., 2000. Ramp function regression: a tool for quantifying climate transitions. Comput. Geosci. 26, 293-307.
- Mudelsee, M., 2009. Break function regression: a tool for quantifying trend changes
- in climate time series. Eur. Phys. J. Spec. Top. 174, 49—63. Nagashima, K., Tada, R., Tani, A., Sun, Y., Isozaki, Y., Toyoda, S., Hasegawa, H., 2011. Millennial-scale oscillations of the westerly jet path during the last glacial period. J. Asian Earth Sci. 40, 1214–1220.
- North Greenland Ice Core Project Members, 2004. High-resolution record of Northern Hemisphere climate extending into the last interglacial period. Nature 431, 147-151.
- Orland, I.J., Edwards, R.L., Cheng, H., Kozdon, R., Cross, M., Valley, J.W., 2015. Direct measurements of deglacial monsoon strength in a Chinese stalagmite. Geology 43, 555-558,
- Pedro, J.B., Markus, J., Christo, B., Feng, H., Stephen, B., Rasmussen, S.O., 2018. Beyond the bipolar seesaw: toward a process understanding of interhemispheric coupling. Quat. Sci. Rev. 192, 27-46.
- Peltier, W., Vettoretti, G., 2014. Dansgaard-Oeschger oscillations predicted in a comprehensive model of glacial climate: a "kicked" salt oscillator in the Atlantic. Geophys. Res. Lett. 41, 7306-7313.
- Porter, S.C., An, Z., 1995. Correlation between climate events in the North Atlantic and China during the last glaciation. Nature 375, 305-308.

- Raisbeck, G., Cauquoin, A., Jouzel, J., Landais, A., Petit, J., Lipenkov, V., Beer, J., Synal, H., Oerter, H., Johnsen, S., Steffensen, J., Svensson, A., Yiou, F., 2017. An improved north—south synchronization of ice core records around the 41 kyr 10 Be peak, Clim. Past 13, 217-229.
- Ramsey, C., 2008. Deposition models for chronological records. Quat. Sci. Rev. 27, 42 - 60
- Rao, Z., Chen, F., Cheng, H., Liu, W., Wang, G., Lai, Z., Bloemendal, J., 2013. Highresolution summer precipitation variations in the western Chinese Loess Plateau during the last glacial. Sci. Rep. 3, 2785. https://doi:10.1038/srep02785.
- Richards. D.A., Dorale, I.A., 2003, Uranium-series chronology and environmental applications of speleothems. Rev. Mineral. Geochem. 52, 407-460.
- Rohling, E., Liu, Q., Roberts, A., Stanford, J., Rasmussen, S., Langen, P., Siddall, M., 2009. Controls on the East Asian monsoon during the last glacial cycle, based on comparison between Hulu Cave and polar ice-core records. Quat. Sci. Rev. 28,
- Schmittner, A., Saenko, O.A., Weaver, A.J., 2003. Coupling of the hemispheres in observations and simulations of glacial climate change. Quat. Sci. Rev. 22,
- Schneider, T., Bischoff, T., Haug, G.H., 2014. Migrations and dynamics of the intertropical convergence zone. Nature 513, 45-53.
- Shackleton, N., Hall, M., Vincent, E., 2000. Phase relationships between millennialscale events 64,000-24,000 years ago. Paleoceanography 15, 565-569.
- Shao, Q., Pons-Branchu, E., Zhu, Q., Wang, W., Valladas, H., Fontugne, M., 2017. High precision U/Th dating of the rock paintings at Mt. Huashan, Guangxi, southern China. Quat. Res. 88, 1–13.
- Shao, Q., Li, C., Huang, M., Liao, Z., Arps, J., Huang, C., Chou, Y., Kong, X., 2019. Interactive programs of MC-ICPMS data processing for ²³⁰Th/U geochronology. Quat. Geochronol. 51, 43-52.
- Sinclair, D.J., Banner, J., Taylor, F.W., Partin, J., Jenson, J., Mylroie, J., Goddard, E., Quinn, T., Jocson, J.M., Miklavič, B., 2012. Magnesium and strontium systematics in tropical speleothems from the Western Pacific. Chem. Geol. 294, 1–17.
- Stocker, T.F., Johnsen, S.J., 2003. A minimum thermodynamic model for the bipolar seesaw. Paleoceanography 18, 1087. https://doi:10.1029/2003PA000920.
- Sun, B., Wang, H., 2015. Analysis of the major atmospheric moisture sources affecting three sub-regions of East China. Int. J. Climatol. 35, 2243–2257.
- Sun, J., 2002. Provenance of loess material and formation of loess deposits on the Chinese Loess Plateau. Earth Planet Sci. Lett. 203, 845–859.
- Svensson, A., Andersen, K.K., Bigler, M., Clausen, H.B., Dahl-Jensen, D., Davies, S.M., Johnsen, S.J., Muscheler, R., Parrenin, F., Rasmussen, S.O., Röthlisberger, R., Seierstad, I., Steffensen, J.P., Vinther, B.M., 2008. A 60000 year Greenland stratigraphic ice core chronology. Clim. Past 4, 47-57.
- Swingedouw, D., Fichefet, T., Huybrechts, P., Goosse, H., Driesschaert, E., Loutre, M.F., 2008. Antarctic ice-sheet melting provides negative feedbacks on future climate warming, Geophys. Res. Lett. 35, 36-44.
- Tan, M., 2014. Circulation effect: response of precipitation $\delta^{18}\text{O}$ to the ENSO cycle in monsoon regions of China. Clim. Dynam. 42, 1067–1077.
- WAIS Divide Project Members, 2015. Precise interpolar phasing of abrupt climate change during the last ice age. Nature 520, 661–665.
- Wang, Q., Zhao, K., Yang, S., Liang, Y., Zhang, J., Cui, Y., Wang, Y., 2020. The response of precipitation $\delta^{18}\text{O}$ in Yongxing cave, Hubei Province to ENSO, 2015. Quat. Sci. 40, 985-991 in Chinese.
- Walczak, M.H., Mix, A.C., Cowan, E.A., Fallon, S.J., Fifield, L.K., Alder, J.R., Du, J., Haley, B.A., Hobern, T., Padman, J., Praetorius, S.K., Schmittner, A., Stoner, J.S., Zellers, S.D., 2020. Phasing of millennial-scale climate variability in the Pacific and Atlantic Oceans. Science 370, 716–720.
- Wang, Y., Cheng, H., Edwards, R., An, Z., Wu, J., Shen, C., Dorale, J.A., 2001. A highresolution absolute-dated late pleistocene monsoon record from Hulu cave, China. Science 294, 2345-2348.
- Warken, S.F., Scholz, D., Spötl, C., Jochum, K.P., Pajón, J.M., Bahr, A., Mangini, A., 2019. Caribbean hydroclimate and vegetation history across the last glacial period. Ouat. Sci. Rev. 218, 75-90.
- Wary, M., Eynaud, F., Rossignol, L., Lapuyade, J., Gasparotto, M., Londeix, L., Malaizé, B., Castéra, M., Charlier, K., 2016. Norwegian Sea warm pulses during Dansgaard-Oeschger stadials: zooming in on these anomalies over the 35-41 ka cal BP interval and their impacts on proximal European ice-sheet dynamics. Ouat Sci Rev 151 255-272
- Weaver, A.J., Saenko, O.A., Clark, P.U., Mitrovica, J.X., 2003. Meltwater Pulse 1A from Antarctica as a trigger of the Bølling-Allerød warm interval. Science 299, 1709-1713.
- Wu, B., Jiang, D., Wang, X., 2021. Changes in the growing season across China during 1961-2018. Chin. J. Atmos. Sci. 45, 424–434.
- Yoshimura, K., Kanamitsu, M., Noone, D., Oki, T., 2008. Historical isotope simulation using Reanalysis atmospheric data. J Geophys. Res. Atm. 113, D19108.
- Zhang, H., Griffiths, M., Huang, J., Cai, Y., Wang, C., Zhang, F., Cheng, H., Ning, Y., Hu, C., Xie, S., 2016. Antarctic link with East Asian summer monsoon variability during the Heinrich Stadial-Bølling interstadial transition. Earth Planet Sci. Lett. 453, 243-251.
- Zhang, P., Cheng, H., Edwards, R., Chen, F., Wang, Y., Yang, X., Liu, J., Tan, M., Wang, X., Liu, J., An, C., Dai, Z., Zhou, J., Zhang, D., Jia, J., Jin, L., Johnson, K.R., 2008. A test of climate, Sun, and culture relationships from an 1810-year Chinese cave record. Science 322, 940-942.
- Zhang, X., Jiang, X., Xiao, H., Cai, B., Yu, T., Shen, C., 2021a. A gradual transition into Greenland interstadial 14 in southeastern China based on a sub-decadally-

resolved stalagmite record. Quat. Sci. Rev. 253, 106769.

Zhang, X., Qiu, W., Jiang, X., Hu, H.-M., Xiao, H., Cai, B., Shen, C., 2021b. Three-phase structure of the east Asia summer monsoon during Heinrich stadial 4 recorded in Xianyun cave, southeastern China. Quat. Sci. Rev. 274, 107267.

Zhang, X., Feng, Y., Zeng, H., Tang, Z., 2021c. Change of NDVi during growing season and its relationship with climate in north China and the adjacent areas from

1982 to 2014. Acta Sci. Nat. Univ. Pek. 57, 153–161.
Zhao, M., Li, H., Shen, C., Kang, S., Chou, C., 2017. δ¹⁸O, δ¹³C, elemental content and depositional features of a stalagmite from Yelang Cave reflecting climate and vegetation changes since late Pleistocene in central Guizhou, China. Quat. Int. 452, 102–115.